PERFORMANCE OF PLL BASED DSGCPS AND FLL CONTROLLED SSGCPS UNDER NORMAL CONDITION AND DIFFERENT GRID FAULTS: A COMPARATIVE STUDY

Saptaparna Basu Roy Chowdhury[1*] – Atanu Maji[1] – Pritam Kumar Gayen[2]

[1] Department of Electrical Engineering, Cooch Behar Government Engineering College, PIN-736170, West Bengal, India
[2] Department of Electrical Engineering, Kalyani Government Engineering College, PIN-741235, West Bengal, India

ARTICLE INFO

***Article history*:**
Received: 09.05.2023.
Received in revised form: 16.07.2023.
Accepted: 30.08.2023.

Keywords:
Double stage grid connected photovoltaic system (DSGCPS)
Single stage grid connected photovoltaic system (SSGCPS)
Phase locked loop (PLL)
Frequency locked loop (FLL)
Total harmonic distortion (THD)

DOI: https://doi.org/10.30765/er.2248

Abstract:

This paper presents two separate studies to address the increasing need for renewable energy sources in the grid to cope with the rising energy consumption. Firstly, a Double Stage Grid Connected Photovoltaic System (DSGCPS) based on Phase Locked Loops (PLL) is developed using Matlab-Simulink. Secondly, a model of a single-stage grid-connected photovoltaic system (SSGCPS) controlled by a frequency locked loop (FLL) is created with comparable environmental parameters and a loading pattern. The research compares the active and reactive power flow dynamics and DC link voltage fluctuations of both systems. Results indicate that the SSGCPS is the preferred option due to its lower hardware requirements. However, it has a lower performance in cases of grid faults compared to DSGCPS. Moreover, the study analyzes the Total Harmonic Distortion (THD) of both models, a crucial factor for performance analysis. The comparative study shows that DSGCPS performs better than SSGCPS during fault in terms of THD. In conclusion, it can be inferred that both models have unique advantages and disadvantages, which are contingent on specific operating conditions.

1 Introduction

As a result of the world's population growth and rapid industrialisation, renewable energy sources have become increasingly important in the modern era. Over the past ten years, power electronics have opened new doors for incorporating renewable sources into the power grid [1]. The most common sources of solar energy used to create electricity are photovoltaic (PV) cells and wind energy [2]; solar energy accounts for a significant portion of the total power produced from all types of sustainable and renewable energy sources [3]. There are various challenges when using renewable energy sources when they are connected to the main power grid, notably for maintaining excellent power quality [4]. This is despite the fact that they are the sole solution to the problem of ever-decaying fossil fuels. Alternating current (AC) electricity is the main source of energy for homes and businesses, whereas solar cells provide direct current. As a result, arrangements are established to convert the DC supply to AC in order to power household and industrial equipment. Additionally, the separate sources and supplies of electricity generation have been replaced by the electricity grid.

Therefore, after being converted to an AC supply, solar electricity must be connected to the grid so as to produce a reliable electrical source. Phase locked loop (PLL) control methods has been employed for a long time to complete the total task. PLL has been widely and successfully employed in the development of automated control systems in a number of sectors. These consist of induction heating power supply [5], electrical motor control systems [6], electronic communication systems [7], etc. PLL approaches are now making it easier to synchronise isolated utility networks with grid-connected inverters [8]. Herein lies the significance of PLL in the context of creating a solar system that is integrated to the grid, which is the main goal of the study suggested here. Since the phase of the incoming power signal and the grid must be synchronised before the isolated supply is connected to the grid, PLL is crucial. However, these systems can

malfunction when faced with load imbalance, harmonic distortion, or frequency changes. Poor DC component and harmonics are problems for the PLL-less approach [9]. In similar systems to PLL where frequency synchronisation is required before connecting the isolated source to the grid, frequency locked loop (FLL) is similarly desirable. Another grid-connected solar energy conversion technique has been developed utilising the Kalman filter [10], but it suffers from high computational complexity, making implementation difficult and expensive.

In the proposed work, a comparative analysis of the performances of a phase locked loop (PLL) based DSGCPS and a frequency locked loop (FLL) controlled SSGCPS have been investigated. Several researchers have worked on the analysis of the single stage and double stage grid connected photovoltaic system. Power loss comparison has been another key factor for the distinction and application of the suitable method. Single stage model has been the less complicated one, whereas, the double stage is intricate in design. The authors of [11] have proposed a study to compare the losses under these two different models: SSGCPS and DSGCPS; although, they have considered several other factors such as voltage ripple due to double line-frequency, variation in the irradiance level, variation in dc loading etc. A single stage scheme involving second-order normalised integrator along with FLL based control has been proposed in [12]. This scheme is also intended towards the mitigation of power quality problems, which often arise, especially for the grid-connected solar PV array. Stability analysis, using non-linear control strategies of single stage grid-connected PV system has been analyzed in [13]; whereas, the authors of [14] have made a stability analysis of double-stage grid-integrated photovoltaic system. A double frequency voltage fluctuation is a major issue in the case of single-phase DC bus capacitor voltage of PV grid-integrated systems. Control schemes for the enhancement of power quality and working efficacy using SSGCPS have been analysed by the researchers of [15]. Management of active and reactive power is another aspect which requires major attention, especially for the grid connected photovoltaic system. The authors of [16] have examined the maximum power point tracking (MPPT) algorithms for PV systems; whereas, the authors of [17] have investigated the behaviour of a three phase single stage grid-connected PV system, installed with MPPT and p–q theory based control strategy, which is very effective in eliminating harmonics from current signals, as used in designing active power filters [18]. A fractional-order (FO) based control scheme has been proposed in [19] for a double stage grid integrated PV system. Several researchers have proposed single-stage inverter schemes for connecting the PV system directly to the grid, ensuring effective transformation of the dc power from the PV cells directly to ac following MPPT [20], [21]. Non-linear sliding mode control has also been experimented with SSGCPS [22]. The paper [23] exclusively focuses on conducting a comprehensive performance analysis of a Double Stage Grid Connected Photovoltaic (DSGCP) system with a non-linear load.

In the suggested work, similar environmental conditions and a loading pattern have been simulated with the help of Matlab-Simulink software. Since the dynamics of the power flow are disturbed by changes in the DC connection voltage, real and reactive power flow have been investigated and compared. A SSGCPS is superior and more cost-effective than the complex DSGCPS model, which introduces double stage analysis, because it has a single stage unit and does not require a PLL or DC-DC converter. However, one of the main goals of our work was to study how the SSGCPS performs when there is a grid fault. Total Harmonic Distortion (THD), a crucial component of performance analysis, is another important element in determining the quality of the alternating power signal. Harmonics are introduced to the output waveform during the initial conversion of the PV-generated DC supply to AC supply using an inverter arrangement, which is also a semiconductor device. This lowers the power quality. Therefore, making an accurate assessment of the signal's quality is crucial. As a result, a comparative research has been created and the two models are also compared in terms of THD. Summarizing our contributions in this work, they are as follows:

- The paper presents a step-by-step implementation of a grid-integrated photovoltaic system with a non-linear load, utilizing both a SRF-PLL based double-stage and an FLL based single-stage configuration.
- Performance analysis of both the single and double-stage models is conducted through simulation in the Matlab/Simulink environment.
- A comparative study is conducted between the two models with respect to various system parameters, like grid current, inverter current, and DC link capacitor voltage variations during normal and different symmetrical and unsymmetrical grid fault conditions.
- The results of the study provide valuable insights into the suitability of the two models under different system conditions, enabling decision-makers to select the appropriate connection type for their specific needs.

2 Methods

2.1 Case study of DSGCPS

2.1.1 Designing of the proposed model

In this instance, the PV system is linked to the three-phase grid in two steps. First stage uses a DC-DC converter, duty ratio of whose is managed by an MPPT controller. By applying adequate control logics, the voltage of the DC link capacitor made to be kept constant. The complete system is then connected to the grid by means of a voltage source inverter (VSC), which converts DC to AC. Frequency and the phase angle of the grid are extracted using a PLL conceptualized on Synchronous Reference Frame (SRF). The primary job is to generate reference current, as well as to obtain gate pulses for the inverter circuit. Figure 1 displays the DSGCPS's complete block diagram.

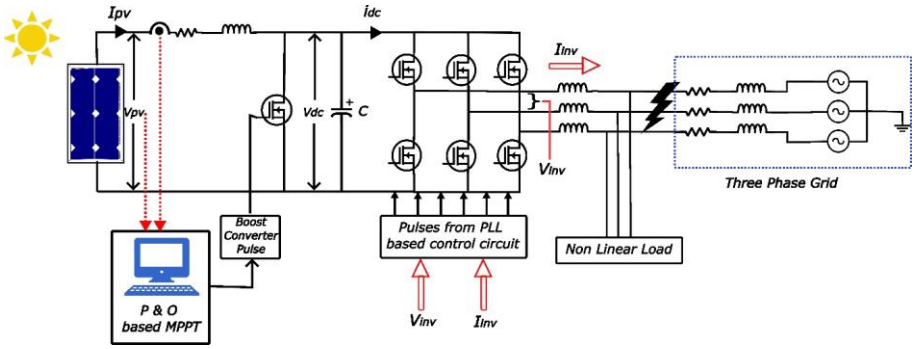

Figure 1. Schematic diagram of overall DSGCPS

Table 1. PV array specifications

Parameter	Value
Number of modules connected in parallel	64
Number of modules connected in series	5
Solar insolation (W/m^2)	1000
Temperature (^oC)	24

Table 2. PV module detail specifications

Parameter	Value
Crest power (W)	314.92
Open Circuit Voltage V_{OC} (V)	65.1
At maximum power point, current I_{mp} (A)	5.67
At maximum power point, voltage V_{mp} (V)	55.1

2.1.2 Control of DC link voltage

Due to the PV cell's non-linear current (I) vs. voltage (V) characteristics, MPPT is constantly required to adjust the operating condition of the PV system in accordance to the weather. By choosing the appropriate duty cycle, MPPT determines the operational PV voltage. To create the proper gate pulse for the IGBT switch of the DC-DC converter, this data is fed through a PWM generator with a 5KHZ switching frequency. Now, for optimal performance, the DC voltage used as the inverter input should be kept constant. The inverter circuit must therefore be connected across an appropriate DC capacitor. In our model, we have selected reference voltage as 700 volts (V_{dref}). DC bus voltage is measured constantly and compared with the pre-set reference voltage. Any deviation from the reference voltage will generate error signal which is then processed through a Proportional and Integral (PI) controller to nullify the said error. Hence DC bus voltage is maintained at pre-set value. PI controller's output is termed as loss power (P_{loss}).

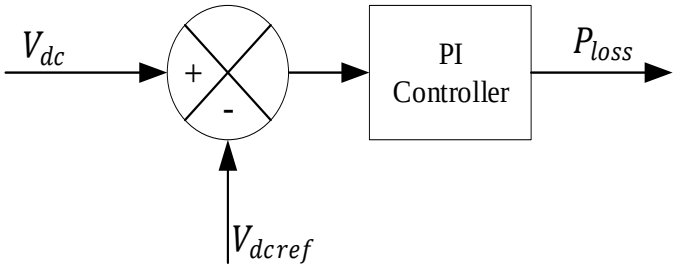

Figure 2. DC bus voltage control

Table 3. Details of P&O MPPT

Parameter	Value
Initial value of duty cycle	0.62
Upper limit of duty cycle	0.8
Lower limit of duty cycle	0.2
Incremental/decremented value of duty cycle	2×10^{-4}
Integrator initial value	0

Table 4. PI Controller specification (both for DSGCPS and SSGCPS)

Parameter	Value
Integral gain	734
Proportional gain	113

2.1.3 Clarke & Park Transformation

Clarke transform deals with the conversion of three phase quantities into an orthogonal components (α and β). These are termed as stationary reference frame variables. Clarke transformation, which is primarily an 'abc to alpha-beta transformation' is given by equations (1) and equations (2) describes the Inverse Clarke transformation (alpha-beta to abc transformation).

$$\begin{bmatrix} i_\alpha \\ i_\beta \\ i_0 \end{bmatrix} = \sqrt{\frac{2}{3}} \begin{bmatrix} 0 & -\frac{1}{2} & -\frac{1}{2} \\ 0 & \frac{\sqrt{3}}{2} & -\frac{\sqrt{3}}{2} \\ \frac{1}{2} & \frac{1}{\sqrt{2}} & \frac{1}{\sqrt{2}} \end{bmatrix} \begin{bmatrix} i_a \\ i_b \\ i_c \end{bmatrix} \tag{1}$$

$$\begin{bmatrix} i_a \\ i_b \\ i_c \end{bmatrix} = \sqrt{\frac{2}{3}} \begin{bmatrix} 1 & 0 & \frac{1}{\sqrt{2}} \\ -\frac{1}{2} & \frac{\sqrt{3}}{2} & \frac{1}{2} \\ -\frac{1}{2} & \frac{\sqrt{3}}{\sqrt{2}} & \frac{1}{\sqrt{2}} \end{bmatrix} \begin{bmatrix} i_\alpha \\ i_\beta \\ i_0 \end{bmatrix} \tag{2}$$

In α-β frame, Φ angle is generated between net voltage vector and α axis. Also net voltage vector is rotating at an angular speed same as the frequency of the measured three phase quantities. If projection of the α-β reference axis components is taken on the rotating reference frame, then the system can be converted to DC. Park transformation is given by equations (3) and (4).

$$\begin{bmatrix} i_d \\ i_q \end{bmatrix} = \begin{bmatrix} \cos\phi & \sin\phi \\ -\sin\phi & \cos\phi \end{bmatrix} \begin{bmatrix} i_\alpha \\ i_\beta \end{bmatrix} \tag{3}$$

By applying inverse park transformation,

$$\begin{bmatrix} i_\alpha \\ i_\beta \end{bmatrix} = \begin{bmatrix} \cos\phi & -\sin\phi \\ \sin\phi & \cos\phi \end{bmatrix} \begin{bmatrix} i_d \\ i_q \end{bmatrix} \tag{4}$$

There can be two types of Park transformations.
If rotating axis frame is allied with phase A axis of the measured signal at t = 0, then d axis component is allied along A axis. It is termed as cosine Park transformation.
And if rotating axis frame is allied 90º behind A axis of the measured signal at t = 0, then q axis component is allied along A axis. It is known as sine Park transformation.
In our study, we have measured phase voltages of the grid and performed sine-based Park transformation which in turn yields the result as q = 0, d = 1, and zero = 0. Hence d axis component of grid voltage i.e. V_d is obtained with the help of Synchronous Reference Frame –PLL which is described below.
3 phase voltage represented by,

$$\begin{bmatrix} V_a \\ V_b \\ V_c \end{bmatrix} = \begin{bmatrix} \cos(\omega t) \\ \cos\left(\omega t - \frac{2\pi}{3}\right) \\ \cos\left(\omega t - \frac{4\pi}{3}\right) \end{bmatrix} V \tag{5}$$

Where, ω is the angular frequency. Therefore, applying Clarke transformation we obtain,

$$\begin{bmatrix} V_\alpha \\ V_\beta \\ V_0 \end{bmatrix} = \sqrt{\frac{2}{3}} \begin{bmatrix} 1 & \cos\frac{2\pi}{3} & \cos\frac{4\pi}{3} \\ 0 & \sin\frac{2\pi}{3} & \sin\frac{4\pi}{3} \\ \frac{1}{\sqrt{2}} & \frac{1}{\sqrt{2}} & \frac{1}{\sqrt{2}} \end{bmatrix} \begin{bmatrix} V_a \\ V_b \\ V_c \end{bmatrix} = V \begin{bmatrix} \cos\omega t \\ \sin\omega t \\ 0 \end{bmatrix} \tag{6}$$

And, applying Park transform, we obtain,

$$\begin{bmatrix} V_d \\ V_q \\ V_0 \end{bmatrix} = \begin{bmatrix} \cos\emptyset & \sin\emptyset & 0 \\ -\sin\emptyset & \cos\emptyset & 0 \\ 0 & 0 & 1 \end{bmatrix} \begin{bmatrix} V_\alpha \\ V_\beta \\ V_0 \end{bmatrix} \tag{7}$$

$$\begin{bmatrix} V_d \\ V_q \\ V_0 \end{bmatrix} = \sqrt{\frac{2}{3}} \begin{bmatrix} \cos\phi & \sin\phi & 0 \\ -\sin\phi & \cos\phi & 0 \\ 0 & 0 & 1 \end{bmatrix} \times \begin{bmatrix} \cos\omega t \\ \sin\omega t \\ 0 \end{bmatrix} V \tag{8}$$

$$\begin{bmatrix} V_d \\ V_q \\ V_0 \end{bmatrix} = \sqrt{\frac{2}{3}} \begin{bmatrix} \cos \omega t \\ \sin \omega t \\ 0 \end{bmatrix} \tag{9}$$

When PLL tracked the voltage vector angle ($\omega t - \Phi$) may be considered as zero. Therefore, for a three phase balanced system quadrature axis component becomes zero when PLL is locked.

2.1.4 Synchronous Reference Frame PLL (SRF-PLL)

Synchronization of the PV system with grid is a major task in which phase angle of the utility grid should be properly assessed with optimum dynamic response. PV inverter performance is dependent on how much accurately this phase angle is measured. There are many existing approaches to find out the phase angle like SRF-PLL, PSD-dq PLL (Positive Sequence Detector based), DSOGI-PLL (Dual Second Order Generalized Integrator). Each method has its own merits and demerits. Among those SRF-PLL has good efficiency in order to track the phase angle (Shah *et al.*, 2018). In our double stage model, we have chosen SRF-PLL. Utility grid's three phase voltages (phase to ground) has been measured and converted into dq0 rotating axis frame (Park transform) by means of an internal oscillator's angular speed. q-axis of the voltage is proportional to the difference in phase between grid voltages in abc form (i.e. ωt) and the rotating frame of internal oscillator (i.e. θ).

$Vq \approx (\omega t - \theta)$

Mean variable frequency block filtered the V_q signal. Automatic gain controlled enabled Proportional-Integral-Derivative (PID) controller makes the phase difference to zero by the help of a controlled oscillator. Thus, the controlled oscillator provides the accurate phase angle of the utility grid which is essential to control the PV inverter.

Thus, we obtain our desired phase angle (ωt) by means of SRF-PLL.

SRF-PLL transfer function can be obtained from the block diagram shown in Figure 3 as follows:

$$TF_{closed} = \frac{TF_{open}}{1 + TF_{open}} \tag{10}$$

Where TF_{open} is the open loop transfer function. Thus, in Laplace domain, we obtain,

$$TF(s) = \frac{T_{PLL}(s)}{S + T_{PLL}(s)} = \frac{V_g(ks + \frac{k}{Ti})}{S^2 + V_g ks + V_g \frac{k}{Ti}} \tag{11}$$

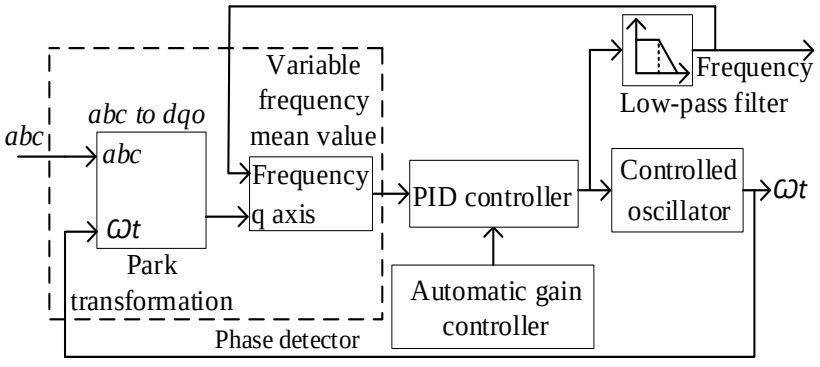

Figure 3. Block diagram of SRF-PLL

Where, V_g represents grid voltage, k is the Proportional gain of low-pass filter (LPF), T_i is the Time constant of integrator of LPF
1/S being the transfer function of the controlled oscillator. Thus, the error of closed loop transfer function becomes as:

$$Err(s) = 1 - TF(s) = \frac{S}{S + T_{PLL}(s)} = \frac{S^2}{S^2 + ks + \frac{k}{Ti}} \tag{12}$$

$$TF(s) = \frac{2\varsigma\omega_n s + \omega_n{}^2}{S^2 + 2\varsigma\omega_n s + \omega_n{}^2} \tag{13}$$

$$\omega_n = \sqrt{\frac{V_g k}{Ti}} \tag{14}$$

$$\varsigma = \sqrt{\frac{V_g kTi}{4}} \tag{15}$$

Where, ζ represents damping ratio of PLL and ω_n stands for natural frequency.

Table 5. Details of SRF-PLL

Parameter	Value
Proportional gain (Kp) of regulator	185
Differential gain (Kd) of regulator	1.00
Integral gain (Ki) of regulator	3250
Rate of change of frequency (maximum) in Hz/sec	12.00
Time constant (Td) for derivative action	0.0001
Filter cut-off frequency used for frequency measurement (Hz)	25
Initial phase angle (degree)	0

2.1.5 Reference current generation

PV maximum power is tracked by means of MPPT tracker and the same has been sensed and termed as P_{PV}. DC link power loss previously measured and denoted as P_{loss}. Hence, actual input DC power to the inverter (P_{Act}) is

$$P_{Act} = (P_{PV} - P_{loss}) \tag{16}$$

By means of SRF-PLL and sine-based Park transformation we have already determined direct axis component of grid terminal voltage i.e. V_d.

Direct axis reference current (I_{dref}) is calculated,

$$I_{dref} = (\tfrac{2}{3} P_{Act}) \,/\, V_d \tag{17}$$

By the help of Inverse Park Transformation, we converted reference d axis current in to phase component i.e. in abc form.

$$I_{dref} \xrightarrow{\text{Inverse Park Transformation}} I_{abc\_ref} \text{ (reference current in abc form)} \quad (18)$$

Thus, reference current in abc form I_{abc_ref} is obtained.

2.1.6 Gate pulse generation

Comparison of I_{abc_ref} is done with PV inverter output current (I_{com}) and generated error signal is passed through hysteresis controller to find out gate pulses for the switches of solar inverter.

2.2 Case study of SSGCPS

2.2.1 Designing of the proposed model

Here PV model is connected to a three phase utility grid via solar inverter only. PV output DC power directly converted into AC by means of VSC inverter and supplies power to the load & grid. MPPT determines the operating voltage of the PV system and accordingly generates DC reference voltage (V_{dref}).

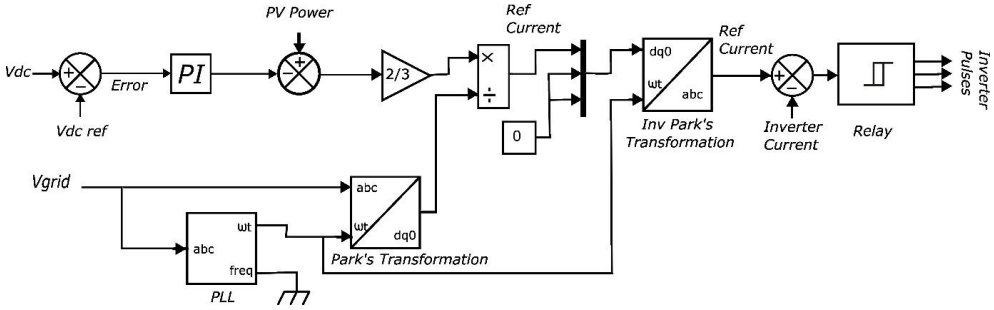

Figure 4. Block diagram of overall control logics of DSGCPS

Here, we have used FLL based control logics for grid synchronization which eliminates the necessity of PLL and DC-DC converter. Due to single stage conversion, it increases complexity in control logic as gate signals of inverter switches has to be chosen in such a way that it not only maintains grid synchronization but also follows the MPPT. Diagram of the overall system is shown schematically in Figure 5.

Table 6. PV array specification

Parameter	Value
Number of module connected in series	25
Number of module connected in parallel	18
Temperature (^oC)	24
Solar insolation (W/m^2)	1000

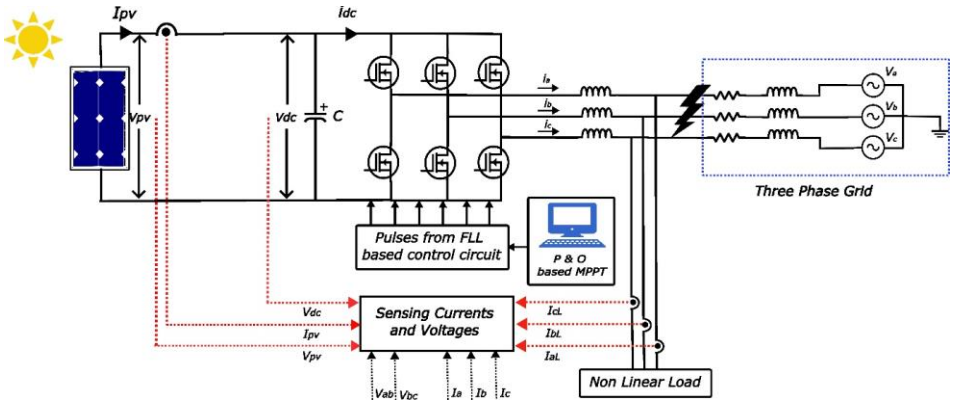

Figure 5. Schematic diagram of overall SSGCPS

Table 7. PV module specification

Parameter	Value
Crest Power (W)	212.15
Open Circuit Voltage V_{OC} (V)	36.4
At maximum power point, current Imp (A)	7.45
At maximum power point, voltage Vmp (V)	29.2

2.2.2 DC bus voltage control and loss current (I_l)

MPPT selects the operational condition of PV system and accordingly generates reference DC voltage (V_{dref}). Actual voltage across DC bus capacitor is measured (V_{dc}) and the same is processed by a first order low pass filter (LPF). Gain of both the voltages i.e. V_{dref} &V_{dc} are attenuated by a factor 1/700 before compared. After comparing error signal has been processed through a PI controller. Thus, DC bus capacitor voltage is controlled by means of suitable PI controller. Any deviation in capacitor voltage from the reference voltage set by MPPT would eventually generates error signal which is processed via PI controller to get DC link loss current (I_l).

$$I_l = (k_p + \frac{k_i}{s})(V_{dcref} - V_{dc}) \tag{19}$$

Where, k_i stands for integral gain and k_p represents proportional gain of PI controller.

Table 8. Details of low pass filter (LPF)

Parameter	Value
Time constant (sec)	10^{-3}
Initial magnitude	0
Initial phase (degree)	0
Initial frequency (Hz)	50

2.2.3 Calculation of Phase voltage (V_a, V_b, V_c), terminal voltage (V_t) and Unit vector voltage (u_a, u_b, u_c) of grid

Line voltages of grid is measured and termed as V_{ab}, V_{bc}, V_{ca}. Now, Phase voltages are calculated by using equation (20).

$$\begin{bmatrix} V_a \\ V_b \\ V_c \end{bmatrix} = \frac{1}{3}\begin{bmatrix} 2 & 1 & 0 \\ -1 & 1 & 0 \\ -1 & -2 & 0 \end{bmatrix}\begin{bmatrix} V_{ab} \\ V_{bc} \\ 0 \end{bmatrix} \tag{20}$$

After calculating phase voltages, we need to find the grid terminal voltage magnitude i.e. V_t which is obtained from equation (21).

$$V_t = \sqrt{\frac{2}{3}(V_a^2 + V_b^2 + V_c^2)} \tag{21}$$

Hence, we have determined both phase voltage and terminal grid voltages. Thus, unit vector voltages may be calculated from equations (22), (23) and (24).

$$u_a = \frac{V_a}{V_t} \tag{22}$$

$$u_b = \frac{V_b}{V_t} \tag{23}$$

$$u_c = \frac{V_c}{V_t} \tag{24}$$

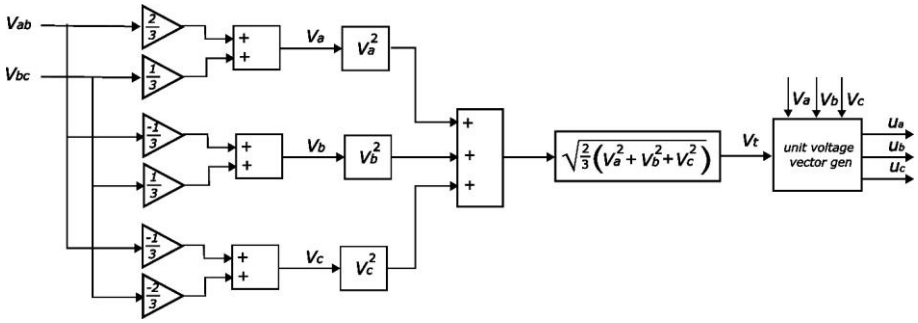

Figure 6. Block diagram of generation of Phase, terminal and unit vector voltages

2.2.4 PV feed forward current (I_{PV})

Maximum DC power tracked continuously by MPPT and is being measured. It is denoted as P_m. Grid terminal voltage $V_t$has already been calculated. Now, feed forward current of PV is obtained with the help of the equation (25)

$$I_{PV} = \frac{2P_m}{3V_t} \tag{25}$$

2.2.5 Calculation of net average load current (I_{load})

Schematic diagram of FLL is presented in Figure 7. FLL controller segregates each phases load current (i_{la}, i_{lb}, i_{ic}) into direct and quadrature axis. For example, load current of phase A (i_{la}) is converted into i_{lad} and i_{laq}. In our FLL structure, we have used the forward Euler method for discrete time integrator. Here, we have considered $\omega_c = 2\times\pi\times50$ Hz = 314 rad/sec.

Calculation of d-q components of phase - a of load current is as follows:

$$I_L(s) = \frac{I_a\omega_1}{s^2+\omega_1^2} + \frac{P}{s} \tag{26}$$

$$I_{lad}(s) = \frac{k_t\omega_1 s}{s^2 + k_t\omega_1 s + \omega_1^2} I_L(s) \tag{27}$$

$$I_{laq}(s) = \frac{k_t s^2}{s^2 + k_t\omega_1 s + \omega_1^2} I_L(s) \tag{28}$$

$$I_{lad}(s) = \frac{k_t\omega_1 s}{s^2 + k_t\omega_1 s + \omega_1^2}\left(\frac{I_a\omega_1}{s^2+\omega_1^2} + \frac{P}{s}\right) \tag{29}$$

$$I_{lad}(s) = I_a \frac{\omega_1}{s^2 + \omega_1^2} + \frac{(k_t P - I_a)}{s^2 + k_t \omega_1 s + \omega_1^2} \tag{30}$$

$$I_{lad}(s) = \frac{k_t \omega_1 s}{s^2 + k_t \omega_1 s + \omega_1^2} \left(\frac{I_a \omega_1}{s^2 + \omega_1^2} + \frac{P}{s}\right) \tag{31}$$

$$I_{laq}(s) = I_a \frac{s}{s^2 + \omega_1^2} + \frac{(k_t P - I_a)s}{s(s^2 + k_t \omega_1 s + \omega_1^2)} \tag{32}$$

$$I_{lad}(t) = I_a \sin(\omega_1 t) + \frac{(k_t P - I_a)}{\sqrt{1 - \frac{k^2}{4}}} e^{\frac{-k_t \omega_1 t}{2}} \sin(\omega_1 t \sqrt{1 - \frac{k_t^2}{4}}) \tag{33}$$

$$I_{laq}(t) = I_a \cos(\omega_1 t) - \frac{(k_t P - I_a)}{\sqrt{1 - \frac{k^2}{4}}} e^{\frac{-k_t \omega_1 t}{2}} \sin(\omega_1 t \sqrt{1 - \frac{k_t^2}{4}} + \cos^{-1}(\frac{k}{2})) \tag{34}$$

Under steady state, DC offset in load current (P) has no adverse effect in the FLL performance (Shah *et al.*, 2018). Hence, FLL based control logic effectively tracks the grid frequency. Now, extracted quadrature components of load current is processed with the help of a sample and hold circuit with the help of unit vector voltages passed by zero crossing detector. Here we have used rising edge trigger for Sample and hold circuit. Output from the sample and hold circuits are denoted as fundamental load currents i.e. i_{laf}, i_{lbf}, i_{lcf}. Hence, net average load current can be estimated as per equation (35).

$$I_{load} = (i_{laf} + i_{lbf} + i_{lcf})/3 \tag{35}$$

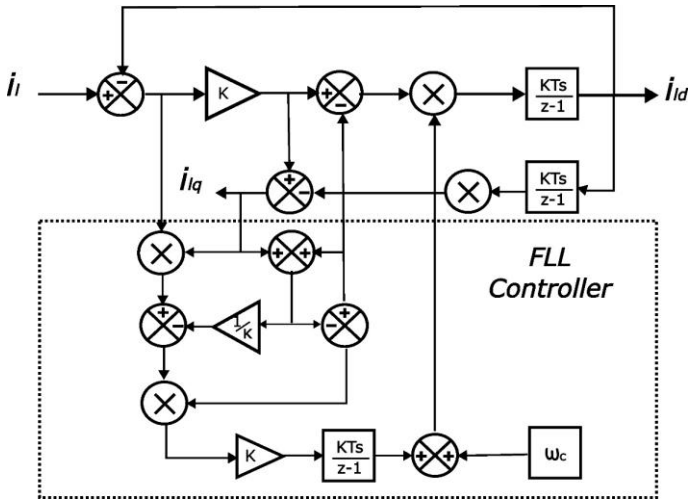

Figure 7. Block diagram of FLL controller

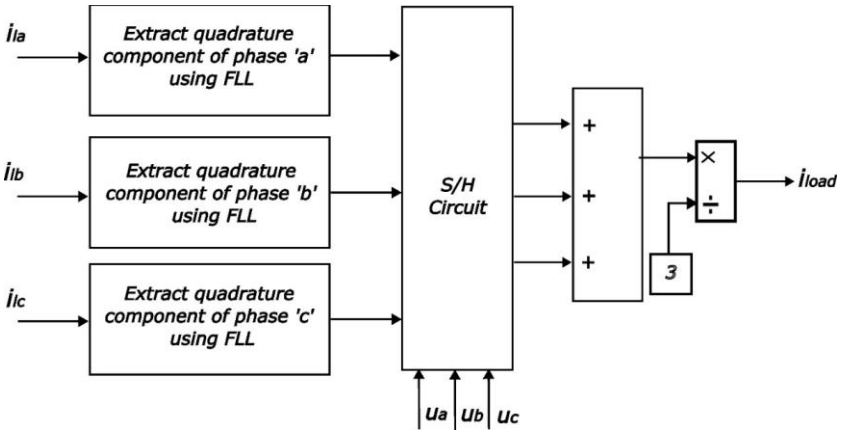

Figure 8. Block diagram of generation of net average load current

2.2.6 Net reference grid current magnitude (I_{net_grid})

Till we have successfully calculated the feed forward current (I_{PV}) of PV system, DC link loss current (I_{dc}) and net load current (I_{load}).
Thus, net value of reference grid current may be obtained as per equation (36)

$$I_{net\_grid} = (I_{PV} - I_l - I_{load}) \tag{36}$$

2.2.7 Actual Reference grid current (I_{aref}, I_{bref}, I_{cref})

Actual reference grid currents for three phases are obtained by multiplying I_{net_grid} with unit grid vector voltages as shown in equations (37), (38) and (39).

$$I_{aref} = u_a * I_{net\_grid} \tag{37}$$

$$I_{bref} = u_b * I_{net\_grid} \tag{38}$$

$$I_{cref} = u_c * I_{net\_grid} \tag{39}$$

Table 9. Details of FLL controller

Parameter	Value/specification
Gain (k)	1000
Angular frequency (ω_c)	314 rad/sec
Integrator type	Discrete
Integrator method	Forward Euler
Integrator initial value	0
Integrator sample time	-1 (-1 for inherited)
S/H circuit trigger type	Rising edge

2.2.8 Gate pulse generation

Finally, inverter output phase currents are measured and compared with calculated actual reference grid currents. Error signal, thus generated, passed through hysteresis current controller to obtain gate pulses for the switches of voltage source inverter.

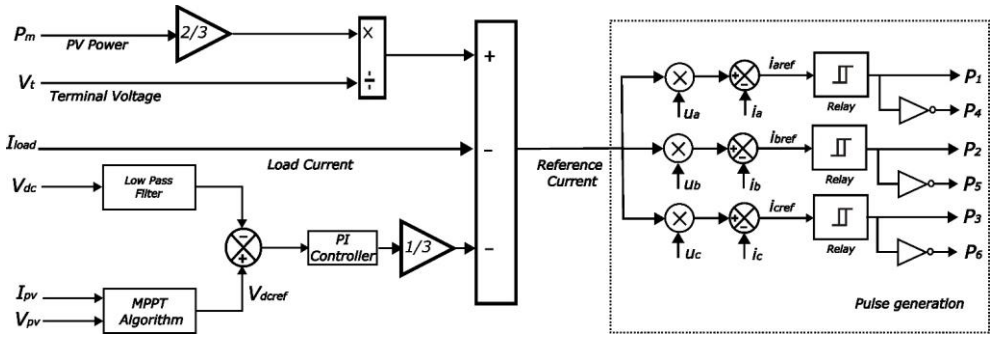

Figure 9. Block diagram of overall control logics of SSGCPS

3 Objectives of the proposed work

We have created both DSGCP and SSGCP model in matlab/Simulink with same non-linear load connected with it. Specification of grid and non-linear load are mentioned in the table 8.Both the model is simulated under normal operating condition keeping same weather conditions i.e. incident solar irradiance and temperature. Next, during the simulation period both the system experienced different types of grid faults. All the output phenomenon were noted and analysed accordingly.

The primary objectives are as follows:
1. Study of DSGCP system during normal operating condition.
2. Study of SSGCP system under normal operating condition.
3. Comparative performance analysis of DSGCP and SSGCP system during normal and various grid faults.

Table 10. Specification of grid

Parameter	Value
Phase-A - phase angle in degree	0
R.M.S value of line to line voltage (Vrms)	400
Short-circuit capacity at base voltage in MVA	100
Frequency in Hz	50
X/R ratio	10

Table 11. Details of Non-linear load (R-L).

Parameter	Value
Resistance in ohm	55
Inductance in henry	0.14×10^{-3}
THD in percentage	22.25

4 Result and discussion

4.1 Results from the study of DSGCPS under normal operating condition

We have established DSGCPS in MATLAB-Simulink. Incident solar irradiance and environment-temperature have been chosen as 1000 W/m^2 and 24 degree C respectively. The system has been made operational for 2 sec. All PV system parameters are shown graphically in Figure 10. MPPT took at around 0.3 sec to track the operating PV voltage. Meanwhile, DC link capacitor voltage also attains its pre-set value of 700 volts. It is observed that PV inverter predominantly supplies active power to the load as well as grid. As the load is basically R-L in nature, hence it needs reactive power also. Reactive power (Var) requirement of the load is mitigated by grid. In our experiment, non-linear load takes around 4.2 KW of active power and around 1.5 KVAR of reactive power. Power flow dynamics of inverter, load and grid is shown in Figure 11.

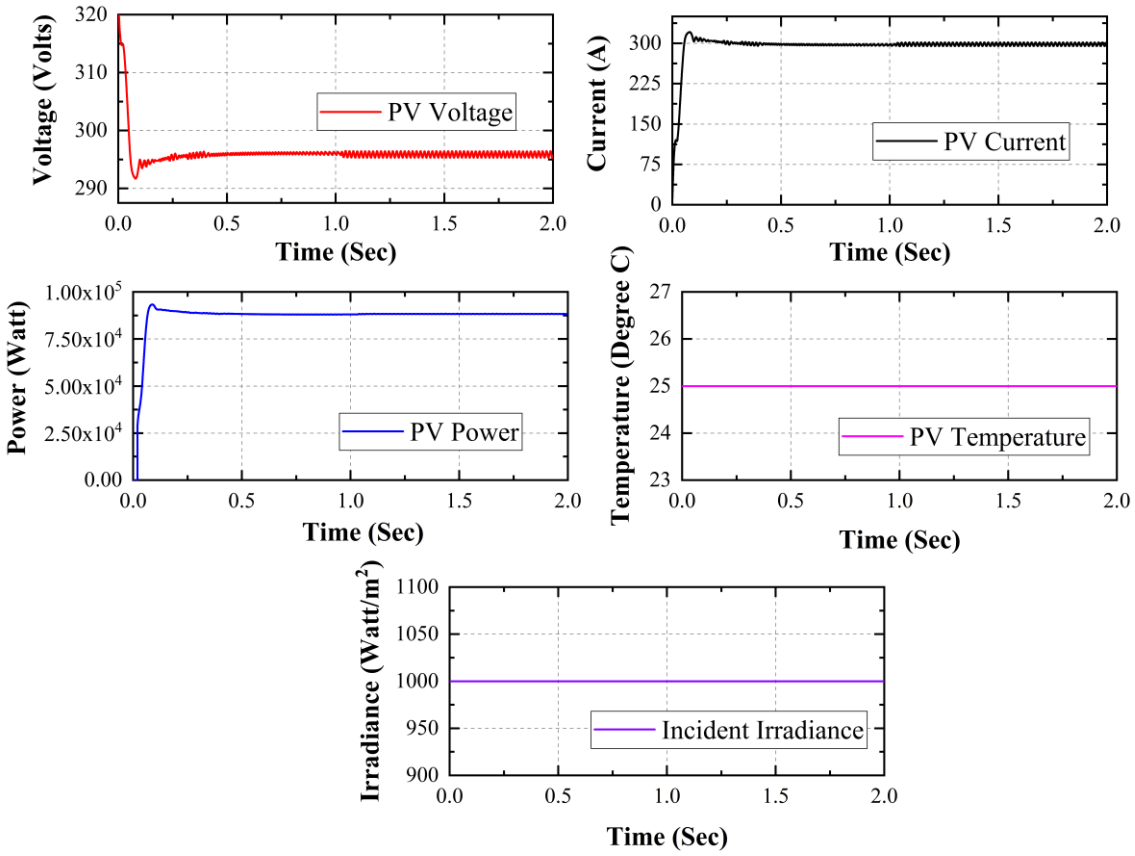

Figure 10. PV voltage, current, power variation with respect to time and temperature & irradiance curve under normal condition of DSGCPS

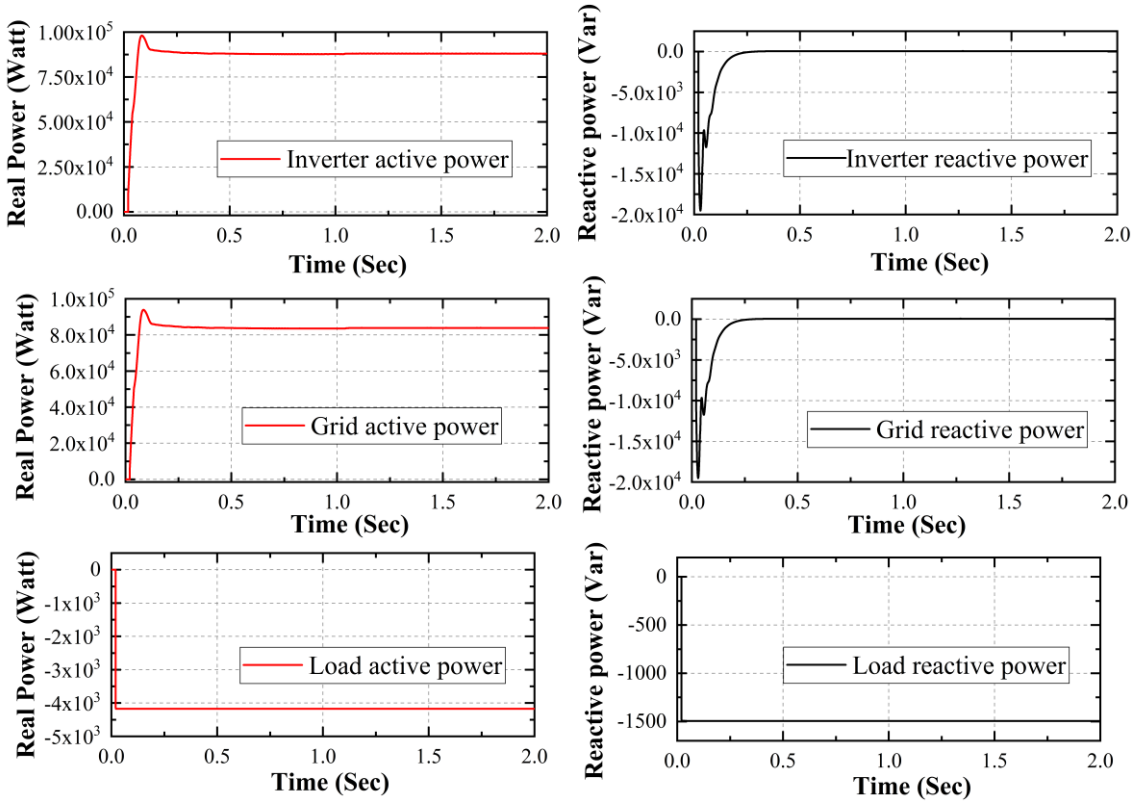

Figure 11. Real and reactive power profiles of Inverter, grid and load under normal condition of DSGCPS

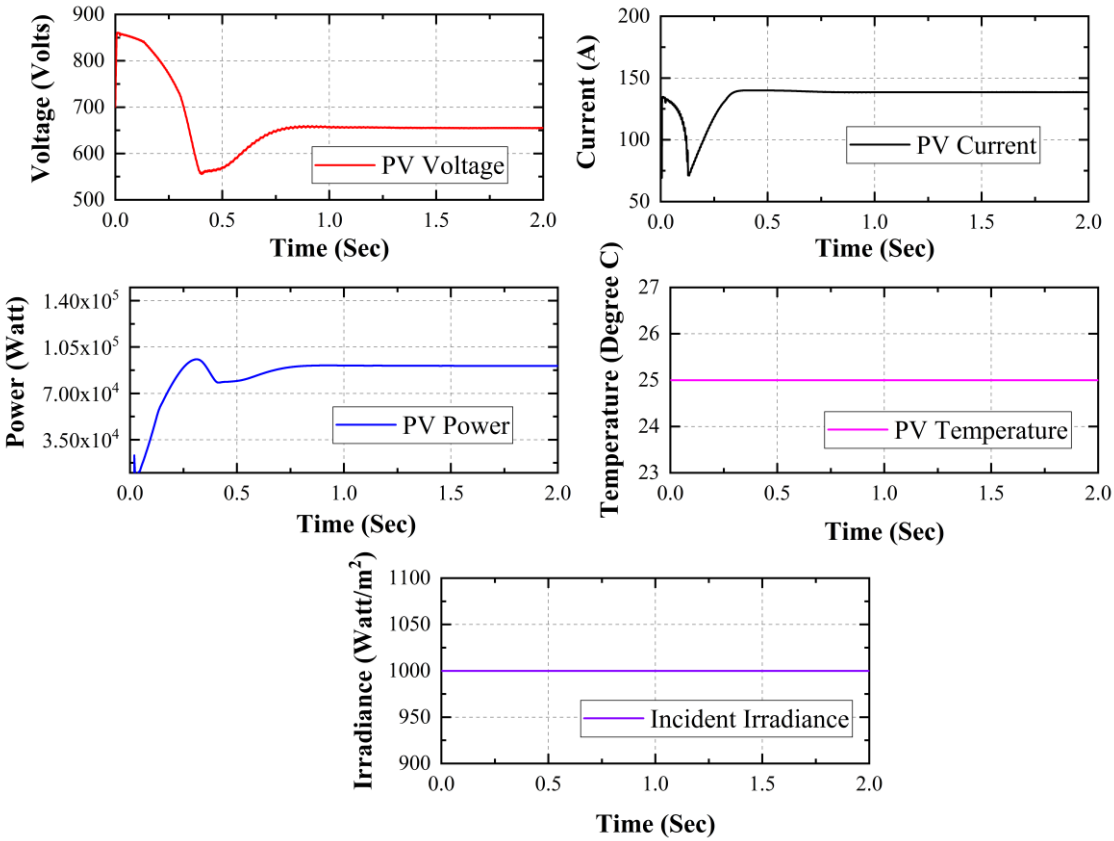

Figure 12. PV current, voltage, power variation with respect to time and temperature & irradiance curve under normal condition of SSGCPS

4.2 Result from study of SSGCPS under normal operating condition

After DSGCP, SSGCP model is created in MATLAB-Simulink. We run the SSGCP model under similar environmental situation as of DSGCP for 2 sec. Here, we noticed that MPPT takes approximately 0.8 sec to track the reference DC voltage which is slightly longer than in case of DSGCPS. In case of SSGCPS model, DC link capacitor voltage will be same as PV voltage. That's why, it took same time i.e. 0.8 sec to stabilize DC link voltage also. Here, PV inverter approximately 91.02 KW of active power in which 86.85 KW is contributed to the grid. Non-linear load consumes 4.17 KW active power which is provided by the PV inverter. Grid feeds the reactive power (Var) to the load which is around 1.49 KVAR. All the responses are shown graphically in Figure 12 and 13.

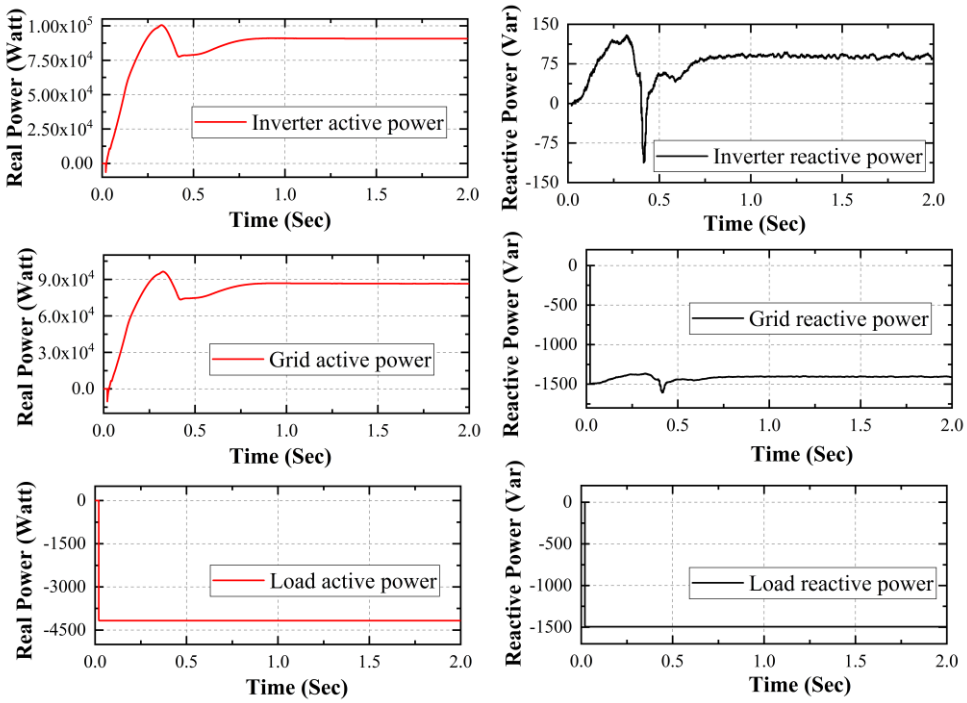

Figure 13. Real and reactive power profiles of inverter, grid and load under normal condition of SSGCPS

4.3 Result from comparative analysis of DSGCPS and SSGCPS during normal condition

After simulating the models in matlab, we calculated THD of inverter and grid current for both the model by means of Fast Fourier Transformation (FFT). Result obtained from FFT shown in Table 10. From Table 10, it is transpired that under normal condition THD values of grid and inverter current are well within the acceptable limit for both the system. If we observe the capacitor voltage profiles, transient decays slightly fast in case of double stage. Figure 14 indicate that for double stage it took about 0.50 sec to stabilize dc link voltage whereas, in case of single stage it took around 0.80 sec.; although, the performance of both the system in accordance to maintaining capacitor voltage is satisfactory.

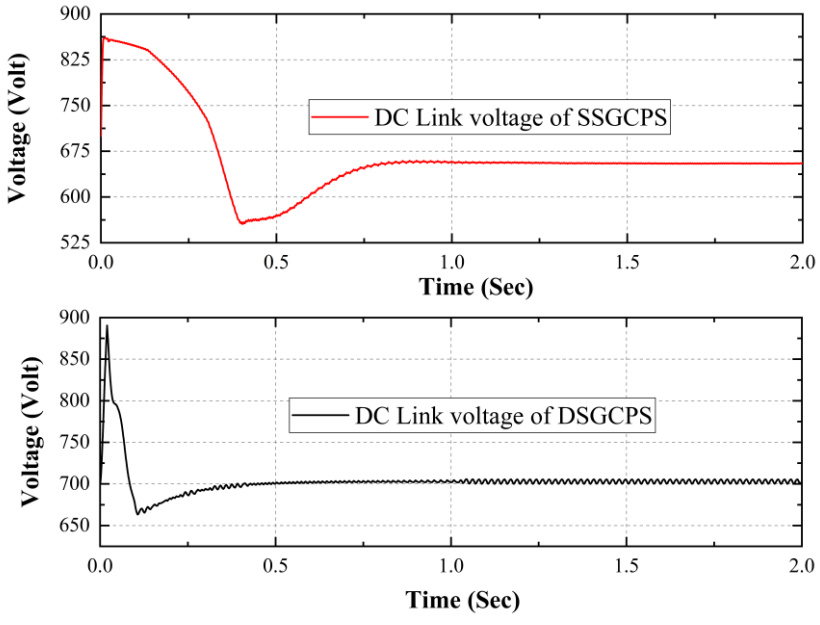

Figure 14. DC link voltage variation of DSGCPS and SSGCPS under normal condition

Table 12. THD values of inverter and grid current of both DSGCPS and SSGCPS

THD of Inverter current		THD of Grid current	
DSGCPS	SSGCPS	DSGCPS	SSGCPS
0.63 %	1.29 %	1.39%	1.79%

4.4 Result from comparative performance analysis of DSGCPS and SSGCPS under various grid faults

In this section we have simulated both double and single stage model for 4 sec. During this period various types of grid fault occurred at t = 2 sec and cleared at t = 3 sec. All types of potential grid faults are considered here. Those are as follows:

- Single line fault (SLG)
- Triple line to ground fault (LLLG)
- Double line to ground fault (LLG)
- Triple line fault (LLL)
- Double line fault (LL)

Here, we made the comparative analysis between the models with respect to two important properties which are described below.

4.4.1 THD of various system currents

THD of grid, inverter and load current is calculated during fault for both single and double stage configuration and plotted graphically as shown in Figure 15. It has been observed that during fault, THD value of inverter and grid current is much higher in single stage model. Load current THD remains almost same for both cases. Another point to be noted that THD values found higher in case of LL and LLG fault in comparison to other types of faults.

4.4.2 DC bus capacitor voltage profile

DC bus voltage profiles for both the models are shown in Figure 16 for all five types of fault. It appears that in case of double stage system DC link voltage quickly attains steady state. During fault duration i.e. from t= 2 – 3 sec capacitor voltage variation is much higher in case of single stage model. Another interesting observation is that capacitor voltage variation is much higher and significant in single stage model in case of LLL and LLLG fault. Overall, it can be apprehended that double stage model has superior performance over single stage in with respect to DC link voltage profile.

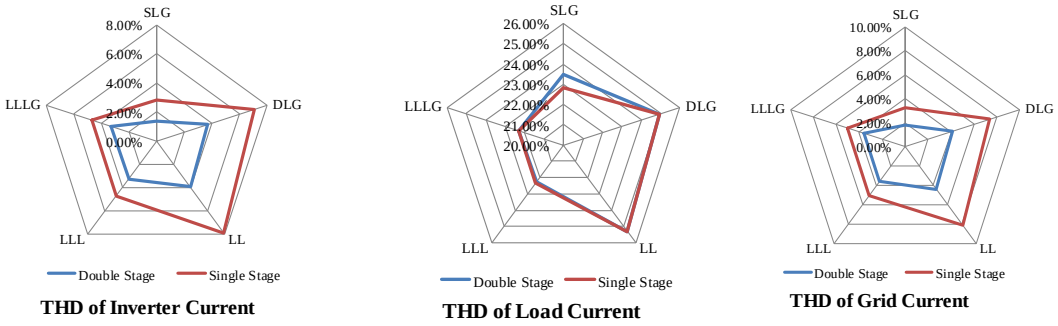

Figure 15. Comparison of inverter, load and grid current THD values of DSGCPS and SSGCPS under various type of grid faults

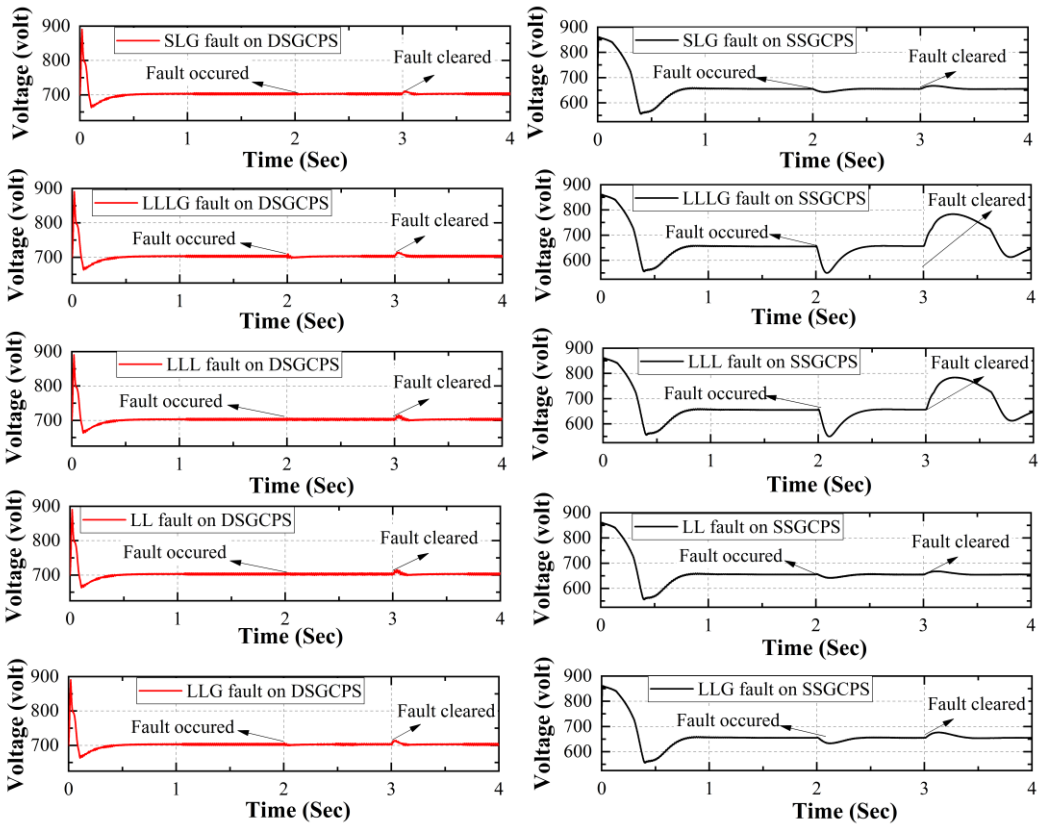

Figure 16. Comparison of DC link voltage variation of (a) DSGCPS and (b) SSGCPS under various type of grid faults

5 Conclusion

Both DSGCPS and SSGCPS ran their simulations in identical circumstances. Both systems operated effectively under typical operational conditions. Although it was well within the permitted limit, the THD value of the grid and inverter current was somewhat greater in the case of SSGCPS. Both systems' DC link voltage profiles were comparatively comparable. The only really significant difference was that it takes slightly longer for SSGCPS to reach steady state. However, SSGCPS has a significant benefit over DSGCPS in that it does not require a PLL or DC-DC converter. Therefore, it can be stated that SSGCPS has an advantage over DSGCPS under typical operating conditions provided there is little variation in tracking time and THD value does not significantly affect the specific system where it will be deployed. On the other hand, during various grid fault situations, it is observed that THD value of inverter and grid current was much higher in case of SSGCPS than DSGCPS system. Specially, in case of SSGCPS during LL and LLG faults, THD values of inverter and grid current were at around 7-8%. As per IEEE 519-2014, if bus voltage is less than 1 KV at the point of common coupling, maximum allowable THD should be under 8%. Thus, DSGCPS has better performance during fault when it comes to THD values. Additionally, it is evident by looking at the DC link voltage profiles for both systems that DSGCPS unquestionably exhibits greater stable reactions and maintains constant DC value during the defective period. On the other hand, SSGCPS saw substantially larger DC voltage variations. Particularly during the LLL and LLLG fault, a large increase in capacitor voltage was observed after the fault had been cleared, and it took time for it to return to the correct level. As a result, it can be said that in defective conditions, PLL-based DSGCPS performs better than FLL-controlled SSGCPS.

Table 13. Symbols and notations

Symbols	Notations
V_{dc}	Measured DC bus voltage
V_{dcref}	Reference DC bus voltage
P_{loss}	Loss DC power
V_a, V_b, V_c	Measured phase voltages of grid
I_a, I_b, I_c	Measured phase currents of grid
V_d, V_q	Direct and quadrature axis voltages
ω	Angular frequency
k	Proportional gain of LPF of SRF-PLL
T_i	Time constant of integrator of LPF
ζ	Damping ratio of PLL
P_{PV}, P_m	MPPT tracked PV power
P_{Act}	DC power input to PV inverter
I_{dref}	Reference direct axis current
I_{abc_ref}	Reference current in phase form
I_l	DC link loss current
K_p, K_i	Proportional and integral gain of PI controller
V_{ab}, V_{bc}, V_{ca}	Measured line voltages of grid
V_t	Terminal grid voltage
u_a, u_b, u_c	Unit vector voltages
I_{PV}	Feed forward PV current
i_{la}, i_{lb}, i_{lc}	Phase values of load current
$i_{laf}, i_{lbf}, i_{lcf}$	Fundamental values of load current
I_{load}	Net average load current
I_{net_grid}	Net value of reference grid current
$I_{aref}, I_{bref}, I_{cref}$	Actual reference grid current

References

[1] F. Iov, M. Ciobotaru, D. Sera, R. Teodorescu, and F. Blaabjerg, "Power Electronics and Control of Renewable Energy Systems," in *2007 7th International Conference on Power Electronics and Drive Systems*, Nov. 2007, p. P-6-P-28. doi: 10.1109/PEDS.2007.4487668.

[2] A. Gupta, S. Chanana, and T. Thakur, "Power quality assessment of a solar photovoltaic two-stage grid connected system: Using fuzzy and proportional integral controlled dynamic voltage restorer approach," *J. Renew. Sustain. Energy*, vol. 7, no. 1, p. 013113, Jan. 2015, doi: 10.1063/1.4906980.

[3] M. A. Eltawil and Z. Zhao, "Grid-connected photovoltaic power systems: Technical and potential problems—A review," *Renew. Sustain. Energy Rev.*, vol. 14, no. 1, pp. 112–129, Jan. 2010, doi: 10.1016/j.rser.2009.07.015.

[4] X. Liang, "Emerging Power Quality Challenges Due to Integration of Renewable Energy Sources," *IEEE Trans. Ind. Appl.*, vol. 53, no. 2, pp. 855–866, Mar. 2017, doi: 10.1109/TIA.2016.2626253.

[5] Q. Zhang, X.-D. Sun, Y.-R. Zhong, M. Matsui, and B.-Y. Ren, "Analysis and Design of a Digital Phase-Locked Loop for Single-Phase Grid-Connected Power Conversion Systems," *IEEE Trans. Ind. Electron.*, vol. 58, no. 8, pp. 3581–3592, Aug. 2011, doi: 10.1109/TIE.2010.2087295.

[6] K. Ding, X. Bian, H. Liu, and T. Peng, "A MATLAB-Simulink-Based PV Module Model and Its Application Under Conditions of Nonuniform Irradiance," *IEEE Trans. Energy Convers.*, vol. 27, no. 4, pp. 864–872, Dec. 2012, doi: 10.1109/TEC.2012.2216529.

[7] A. Chatterjee, A. Keyhani, and D. Kapoor, "Identification of Photovoltaic Source Models," *IEEE Trans. Energy Convers.*, vol. 26, no. 3, pp. 883–889, Sep. 2011, doi: 10.1109/TEC.2011.2159268.

[8] S. Natesan and J. Venkatesan, "A SRF-PLL Control Scheme for DVR to Achieve Grid Synchronization and PQ Issues Mitigation in PV Fed Grid Connected System," *Circuits Syst.*, vol. 07, no. 10, pp. 2996–

3015, 2016, doi: 10.4236/cs.2016.710256.

[9] B. Singh, C. Jain, S. Goel, A. Chandra, and K. Al-Haddad, "A Multifunctional Grid-Tied Solar Energy Conversion System With ANF-Based Control Approach," *IEEE Trans. Ind. Appl.*, vol. 52, no. 5, pp. 3663–3672, Sep. 2016, doi: 10.1109/TIA.2016.2582141.

[10] R. Panigrahi and B. Subudhi, "Performance Enhancement of Shunt Active Power Filter Using a Kalman Filter-Based Control Strategy," *IEEE Trans. Power Electron.*, vol. 32, no. 4, pp. 2622–2630, Apr. 2017, doi: 10.1109/TPEL.2016.2572142.

[11] T.-F. Wu, C.-H. Chang, L.-C. Lin, and C.-L. Kuo, "Power Loss Comparison of Single- and Two-Stage Grid-Connected Photovoltaic Systems," *IEEE Trans. Energy Convers.*, vol. 26, no. 2, pp. 707–715, Jun. 2011, doi: 10.1109/TEC.2011.2123897.

[12] P. Shah, I. Hussain, and B. Singh, "Single-Stage SECS Interfaced With Grid Using ISOGI-FLL-Based Control Algorithm," *IEEE Trans. Ind. Appl.*, vol. 55, no. 1, pp. 701–711, Jan. 2019, doi: 10.1109/TIA.2018.2869880.

[13] M. Aourir, A. Abouloifa, I. Lachkar, C. Aouadi, F. Giri, and J. M. Guerrero, "Nonlinear control and stability analysis of single stage grid-connected photovoltaic systems," *Int. J. Electr. Power Energy Syst.*, vol. 115, p. 105439, Feb. 2020, doi: 10.1016/j.ijepes.2019.105439.

[14] L. Huang, D. Qiu, F. Xie, Y. Chen, and B. Zhang, "Modeling and Stability Analysis of a Single-Phase Two-Stage Grid-Connected Photovoltaic System," *Energies*, vol. 10, no. 12, p. 2176, Dec. 2017, doi: 10.3390/en10122176.

[15] M. Salem and Y. Atia, "Control scheme towards enhancing power quality and operational efficiency of single-phase two-stage grid-connected photovoltaic systems," *J. Electr. Syst. Inf. Technol.*, vol. 2, no. 3, pp. 314–327, Dec. 2015, doi: 10.1016/j.jesit.2015.05.002.

[16] S. B. R. Chowdhury, A. Mukherjee, and P. K. Gayen, "Maximum power point tracking of photovoltaic system by Perturb & Observe and Incremental Conductance methods under normal and partial shading conditions," in *2021 Innovations in Energy Management and Renewable Resources(52042)*, Feb. 2021, pp. 1–6. doi: 10.1109/IEMRE52042.2021.9386964.

[17] G. Tsengenes and G. Adamidis, "Investigation of the behavior of a three phase grid-connected photovoltaic system to control active and reactive power," *Electr. Power Syst. Res.*, vol. 81, no. 1, pp. 177–184, Jan. 2011, doi: 10.1016/j.epsr.2010.08.008.

[18] L. S. Czarnecki, "Currents' Physical Components (CPC) in Circuits with Nonsinusoidal Voltages and Currents. Part 2: Three-Phase Three-Wire Linear Circuits," *Electr. Power Qual. Util.*, vol. 12, no. 1, pp. 3–13, 2006.

[19] S. Fahad, N. Ullah, A. J. Mahdi, A. Ibeas, and A. Goudarzi, "An Advanced Two-Stage Grid Connected PV System: A Fractional-Order Controller," Apr. 2020.

[20] S. Jain and V. Agarwal, "A Single-Stage Grid Connected Inverter Topology for Solar PV Systems With Maximum Power Point Tracking," *IEEE Trans. Power Electron.*, vol. 22, no. 5, pp. 1928–1940, Sep. 2007, doi: 10.1109/TPEL.2007.904202.

[21] Wu Libo, Zhao Zhengming, and Liu Jianzheng, "A Single-Stage Three-Phase Grid-Connected Photovoltaic System With Modified MPPT Method and Reactive Power Compensation," *IEEE Trans. Energy Convers.*, vol. 22, no. 4, pp. 881–886, Dec. 2007, doi: 10.1109/TEC.2007.895461.

[22] M. D. and V. Sankaranarayanan, "A novel nonlinear sliding mode controller for a single stage grid-connected photovoltaic system," *ISA Trans.*, vol. 107, pp. 329–339, Dec. 2020, doi: 10.1016/j.isatra.2020.07.021.

[23] S. B. R. Chowdhury, A. Maji, P. K. Gayen, and S. K. Chowdhury, "Performance analysis of PLL based DSGCP (Double Stage Grid Connected Photovoltaic) system with non-linear load under normal and various grid fault conditions," in *2022 IEEE International Conference of Electron Devices Society Kolkata Chapter (EDKCON)*, Nov. 2022, pp. 29–34. doi: 10.1109/EDKCON56221.2022.10032926.